



Cell–substrate traction force regulates the fusion of osteoclast precursors through cell–cell interaction

Qing Sun¹ · Chengling Liu¹ · Xue Bai¹ · Bo Huo¹ 

Received: 11 June 2019 / Accepted: 27 August 2019 / Published online: 16 September 2019
© Springer-Verlag GmbH Germany, part of Springer Nature 2019

Abstract

The adhesion morphology of a cell monolayer results in a mechanical force inside cells, between cells, or between cells and substrates. The mechanical force regulates the differentiation of stem cells, but its influence on cell fusion is seldom studied. The present study is focused on osteoclast precursors, RAW264.7 monocytes, which can fuse into multinucleated cells (MNCs) responsible for bone resorption. Cells were cultured on circular and ring-like patterned substrates. Then, cell fusion, cell–substrate traction force, and force-sensitive molecules in different regions were measured and analyzed. Results showed that MNCs mainly appeared in the interior of the ring-like pattern and the central zone of the circular pattern, where both cell–substrate traction force and in-plane maximal shear stress were smaller than that at the patterns' edge. The immunostaining results revealed that F-actin, vinculin, β -catenin, and E-cadherin were highly distributed at the edge of patterns. High seeding density of cells promoted mechanical force-dependent fusion. When calcium-dependent cell–cell connections were inhibited by E-cadherin antibody or low-calcium medium, the fusion into MNCs was greatly reduced. Thus, the morphology of cell monolayer decides the mechanical state of cell–substrate interaction and cell–cell connection, ultimately regulating the fusion of osteoclast precursors.

Keywords Osteoclast precursor · Fusion · Micropattern · Cell–cell connection · Cell–substrate interaction

1 Introduction

The *in vivo* morphology of biological tissues is very important for tissue morphogenesis, remodeling, and regeneration (Kim et al. 2014; Hashimoto and Munro 2018; Merle and Farge 2018; Vuong-Brender et al. 2017). The adhesion morphologies of stem cells regulate cell differentiation through cell–matrix interactions and finally determine tissue morphology (Fu et al. 2013; Kilian et al. 2010; McBeath et al.

2004). For example, when epidermal stem cells are seeded on collagen-coated rings with central non-adhesive disks, differentiation only occurs at the center region where the cell–cell adhesive interaction is much stronger (Gautrot et al. 2012). After having been cultured on circular patterns, the human mesenchymal stem cells located at the edges tend to undergo osteogenesis, whereas those at the center differentiate into adipocytes (Wan et al. 2010; Ruiz and Chen 2008).

This adhesion-dependent cell differentiation may be due to the distribution of mechanical state in a cell monolayer, which correlates with the adhesion morphology. Traction force analysis revealed that the regions with high cell–matrix shear stress result in the osteogenesis of stem cells, whereas regions with low shear stress result in differentiation of adipocytes (Anderegge et al. 2011). Cell proliferation occurs at the edge of a circular pattern or the corner regions of a rectangular pattern, where high traction stress is generated within the cell sheet (Nelson et al. 2005). In addition, when cell–cell interaction is inhibited by blocking the binding of E-cadherin to β -catenin, the concentrated proliferation is substantially reduced. However, more evidences on the

Qing Sun, Chengling Liu, Xue Bai are contributed equally to this work.

Electronic supplementary material The online version of this article (<https://doi.org/10.1007/s10237-019-01223-4>) contains supplementary material, which is available to authorized users.

✉ Bo Huo
huobo@bit.edu.cn

¹ Biomechanics Lab, Department of Mechanics, School of Aerospace Engineering, Beijing Institute of Technology, No. 5 South Zhongguancun Street, Beijing 100081, People's Republic of China

relationship among mechanical state, cell differentiation, and the morphology of cell monolayer are still needed to clarify the mechanism of tissue morphogenesis, remodeling, and regeneration.

Osteoclasts are highly specialized multinucleated cells (MNCs) that are uniquely capable of resorbing the bone matrix. The formation of mature osteoclasts is characterized by the fusion of mononuclear phagocytes (i.e., osteoclast precursors) originating from hematopoietic stem cells. The differentiation process is induced by cytokines such as macrophage colony-stimulating factor and receptor activator of NF- κ B. Apart from these chemical factors, mechanical factors such as membrane tension or cytoskeletal dynamics play important roles in the fusion process (Shillcock and Lipowsky 2005; Kozlov et al. 2010). In addition, the cell–cell interaction prior to the fusion mediated by cadherin, a calcium-dependent adhesion molecule, is also important for cell fusion (Mbalaviele et al. 1995; Helming and Gordon 2009). Bone resorption is characterized by a specific structure named bone multinucleated unit, in which osteoclast precursors aggregate at the tip of the cutting zone in a resorption tunnel. However, the mechanism of osteoclast precursors' fusion in this region is still unknown.

In the present work, we measured the cell–substrate traction force in the monolayer of osteoclast precursors, RAW264.7 monocytes, which were cultured on ring-like or circular patterns and analyzed the effect of cell monolayer's morphology on cell fusion. The fused MNCs largely occurred in the interior of the ring-like pattern, which was consistent with the mechanical state. Furthermore, inhibiting

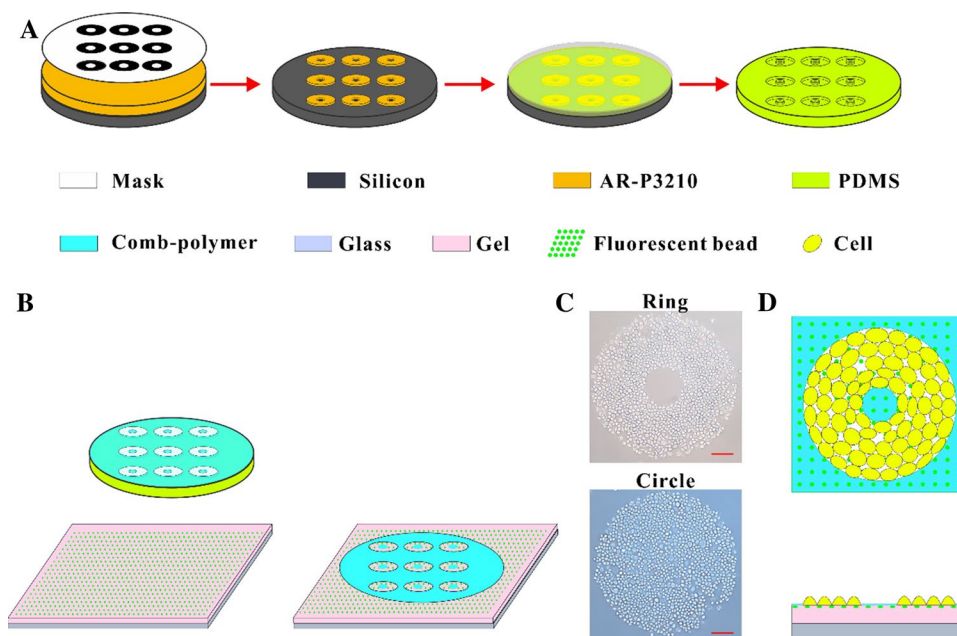
cell–cell interaction significantly reduced this region-dependent cell fusion.

2 Materials and methods

2.1 Micropatterning of substrate

The micropatterned substrate was obtained by soft lithography. Briefly, a mask with geometrically designed features (Fig. 1a) was first fabricated, including the circular pattern with radius 350 μ m and the ring-like pattern with inner radius 100 μ m and outer radius 350 μ m. Then, the features were replicated on the layer of the positive AR-P3210 photoresist (ALLRESIST, Germany) with 5 μ m thickness on a silicon wafer by exposing the photoresist to UV radiation. The PDMS mixed with Dow Corning 184 gel and curing agent (Dow Corning, USA) was poured onto the master in a petri dish. Then, it was vacuumed for 2 h and permitted to cure at 60 $^{\circ}$ C for 8 h. The PDMS stamp was washed with acetone and alcohol and then treated with oxygen ion sputtering to become hydrophilic. The comb polymer (Suzhou Nanotechnology Institute, China), which is non-adhesive to proteins or cells, was used to make the micropatterned substrate (Ma et al. 2005). One droplet of comb polymer solution was placed onto the stamp surface and was made uniform by centrifuging at 600 rpm for 10 s and 2500 rpm for 20 s (Fig. 1b). The stamp with the comb polymer was immediately impressed onto a slide with pre-coated type I collagen (Sigma, USA). The micropatterned slide was

Fig. 1 Cell seeding on the micropatterned substrate. **a** Schematic graph of the fabrication of PDMS stamp. **b** Soft lithography on a fluorescent bead-embedded gel layer with PDMS stamp. **c** Photographs of RAW264.7 cells cultured on the circular and ring-like micropatterned substrates. **d** Schematic graph of cell seeding on the ring-like micropatterned surface



immersed in phosphate-buffered saline (PBS) for 2 h and sterilized by UV light for 2 h before seeding cells.

2.2 Traction force measurement

The polyacrylamide substrate was prepared to measure the traction force between the cell monolayer and substrate. Briefly, NaOH solution was dropped on a glass slide to cover the surface (Sinopharm Chemical Reagent, China) and then air-dried at room temperature. Furthermore, 3-aminopropyltrimethoxysilane (Sigma, USA) was smeared uniformly on the glass surface. After being treated for 5 min, the glass slide was washed thrice with distilled water and was then incubated with 0.5% glutaraldehyde (Sinopharm Chemical Reagent, China) for 30 min. Acrylamide, distilled water, and N,N-methylenebis (Bio-Rad, USA) were mixed with fluorescent beads (Sigma, USA) at a certain proportion (133:243:24:3.3). The mixture was then vibrated in an ultrasonic machine for approximately 5 min. *N,N,N,N*-Tetramethylethylenediamine (Sinopharm Chemical Reagent, China) was added into the solution and mixed evenly. The mixed solution (50 mL) was dropped onto a blank coverslip, which further covered the activated surface of glass slide. This sandwich structure was inverted for 30 min, and the coverslip was removed to form a gel with 100 μm thickness. The stiffness of the polyacrylamide substrate is 30 kPa (Robert et al. 1997). The surface of the gel substrate was washed with HEPES and covered with Sulfo-SANPAH (Pierce Chemical, USA) under UV irradiation for 30 min. Then, 300 μL of type I collagen (Sigma, USA) solution was coated on the substrate and stored at 4 $^{\circ}\text{C}$ overnight. The gel substrate was washed extensively with PBS and then dried off at room temperature. Similar to the process mentioned before, the micropattern feature was transferred on this surface and then incubated with a culture medium for 2 h before seeding cells (Fig. 1b).

To measure the traction force, the deformation of the substrate should be recorded. Briefly, the cells were seeded on the substrate and then cultured for 2, 4, or 6 days. Then, an initial fluorescent image of the beads was recorded, followed by capturing another image of the beads after trypsinizing cells from the substrate. Based on the two consecutive fluorescent images, the displacement field in the substrate was calculated by using digital image correlation. Finally, constrained Fourier transform traction cytometry was used to calculate the traction force based on the displacement field.

2.3 Finite element analysis

To further investigate the mechanical state in a cell monolayer with different patterns, two finite element models mimicking circular and ring-like patterns were built. The cell monolayer was assumed to be a homogeneous elastic solid,

considering that the cells were connected with each other by cell–cell junction. The substrate was also regarded as a homogenous elastic solid connected with a cell monolayer due to the tight junction between cells and substrates by focal adhesion. The radius of a cell monolayer on a circular or ring-like pattern was 350 μm , and the height was 10 μm . The side length of a square substrate was 800 μm , and the height was 50 μm . Tetrahedral elements were adopted for both models (Fig. 3a, b), and the elements' size at the interface between cell monolayer and substrate was approximately 0.28 μm , consistent with or smaller than that of the focal adhesion complex (He et al. 2015). The contractility of a cell monolayer was simulated by a thermal contraction with a thermal expansion coefficient of 10^{-1}K^{-1} (Liu et al. 2016; He et al. 2014). Elastic modulus and Poisson's ratio were 50 kPa and 0.45 for the cell monolayer and 30 kPa and 0.4 for the substrate, respectively (He et al. 2015). The bottom of the substrate was fixed. The above numerical simulation was performed with the COMSOL software.

2.4 Cell culture and inhibition of cell–cell connection

The osteoblast-like MC3T3-E1 cell line was purchased from the American Type Culture Collection (USA) and cultured in alpha-modified Eagle medium (Hyclone, USA) supplemented with 10% fetal bovine serum (FBS; Gibco, USA), 100 U/mL of penicillin (Sigma, USA), and 100 U/mL of streptomycin (Sigma, USA). The medium was changed every 48 h, and the conditioned medium was collected every 24 h when cells reached 70% confluence. The RAW264.7 cell line was purchased from the European Collection of Cell Cultures (UK) and cultured in Dulbecco's modified Eagle medium (DMEM; Hyclone, USA) supplemented with 10% FBS, 100 U/mL of penicillin, and 100 U/mL of streptomycin. After reaching 80% confluence, the RAW264.7 cells were resuspended and then seeded on the micropatterned substrate (Fig. 1c, d) with a high density of 1400 cells/ mm^2 (HD) or low density of 300 cells/ mm^2 (LD).

As described in our previous study (Li et al. 2012), the mononucleated RAW264.7 cells were induced for 2, 4, or 6 days to fuse or differentiate into multinucleated osteoclasts with 1:1 mixture of fresh DMEM with the conditioned medium from osteoblast-like MC3T3-E1 cells. For the low-calcium group, DMEM was replaced with calcium-free DMEM (Gibco, USA), and the final calcium concentration in the medium was 0.9 mM. To inhibit the cell–cell interaction through E-cadherin, anti-E-cadherin antibody ECCD-1 (Takara Bio, Japan) was kept in the induction medium.

2.5 Fluorescent staining of force-transmitting molecules

Several types of molecules responsible for transmitting intracellular, intercellular, or cell–substrate interaction were fluorescently stained to display their distribution in the cell monolayer. RAW264.7 cells were seeded on confocal dishes with micropatterned substrate. After 4-day induction with conditioned medium, cells were rinsed thrice with PBS, then fixed with 4% paraformaldehyde (Beijing Chemical, China) for 30 min, and permeabilized in 0.1% Triton X-100 (Xilong Chemical, China) for 20 min. To fluorescently stain F-actin, cells were treated with phalloidin (Alexis Biochemicals, Switzerland) at 1:100 dilution with PBS for 1 h at 37 °C. For staining vinculin, cells were first blocked with 5% rabbit serum (Beijing ComWin Biotech, China) for 30 min and then rinsed thrice with PBS. Afterward, they were incubated with anti-mouse vinculin antibody (Santa Cruz, USA) at 1:100 dilution with rabbit serum overnight at 4 °C. After being rinsed thrice with PBS, cells were incubated with anti-sheep IgG antibody (Beijing ComWin Biotech, China) for 2 h at 37 °C. To stain β -catenin, cells were blocked with 1% BSA (BOSTER, China) for 30 min, and after being rinsed thrice with PBS, they were incubated with anti-mouse β -catenin antibody (Cell Signaling Technology, USA) at 1:100 dilution with 1% BSA overnight at 4 °C. After being rinsed thrice with PBS, anti-rabbit IgG antibody (Beijing ComWin Biotech, China) at 1:50 dilution with 1% BSA was incubated with cells for 22 h at 37 °C. For E-cadherin staining, cells were blocked with 1% BSA for 30 min and then rinsed thrice with PBS. Then, they were incubated with anti-mouse E-cadherin antibody DECMA-1 (Abcam, UK) at 1:100 dilution with 1% BSA overnight at 4 °C. After being rinsed thrice with PBS, cells were incubated with anti-Rat IgG antibody of Alexa Fluor[®] 488 Conjugate (Cell Signaling Technology, USA) at 1:200 dilution with 1% BSA for 2 h at 37 °C. After fluorescent staining, cells were incubated with Hoechst 33342 (Molecular Probes, USA) for 15 min to stain cell nuclei. A Leica confocal microscope was used to record fluorescent images.

2.6 Identification of cell fusion

Cells were washed with PBS (Hyclone, USA) twice after removing the culture medium and fixed with citrate–acetone solution (25:65:8 for citrate/acetone/methanol) for 30 s at room temperature. Then, cells were incubated with TRAP staining kit (Sigma, USA) reaction solution at 37 °C for 1 h in the dark. After being washed with deionized water thrice, cells were incubated with 0.2 mM Hoechst (Invitrogen, USA) for 10 min, followed by washing with PBS twice. A Leica DMI 6000B inverted microscope was used to capture the fluorescent images.

2.7 Data analysis

To evaluate the effect of adhesion profile on the fusion of osteoclast precursors in the ring-like pattern group, six regions were divided uniformly along a radial direction. For the circular pattern, eight regions were divided along the radial direction. We also determined the cells' location by the bright field, and the number of nuclei was determined by fluorescence staining. In addition, the radial distribution of force-transmitting molecules in ring-like pattern was obtained by calculating the average gray value in each region after background subtraction. All experiments were performed at least six times, and more than 1500 cells were measured for each group. The data were presented as mean \pm standard deviation unless stated otherwise. One-way analysis of variance with Bonferroni's post hoc analysis was performed to determine the statistical significance of the differences between the mean values of different groups ($P < 0.05$).

3 Results

3.1 Fusion of osteoclast precursors depends on the adhesion morphology of cell monolayer

The RAW264.7 cells were seeded on ring-like or circular patterns. Then, the cells were grown to a monolayer with the conditioned medium from MC3T3-E1 osteoblasts for 2, 4, or 6 days. The cells were stained using the TRAP kit and Hoechst (Fig. 2a) to visualize the differentiation of osteoclast precursors. The region occupied by each cell was determined by the bright-field images, and cell fusion was analyzed by calculating the number of nuclei in each region. For the circular pattern group after 2-day culture, the proportion of MNCs decreased with the distance away from the center (Fig. 2b). The highest proportion appeared at the center region (approximately 3.6%), and the lowest at the periphery region (approximately 1%), but no significant difference among different regions was detected. After 6-day culture, the proportion in the center reached 8.3%, which was significantly higher than that in other regions. For the ring-like pattern group, the fusion proportion also increased with time, and the highest value was located in the interior region rather than in the edge region (Fig. 2c).

3.2 Numerical simulation reveals the region-dependent distribution of traction force

We assume that the above region-dependent fusion of osteoclast precursors might correlate with the mechanical state in the cell monolayer. Therefore, numerical analyses were

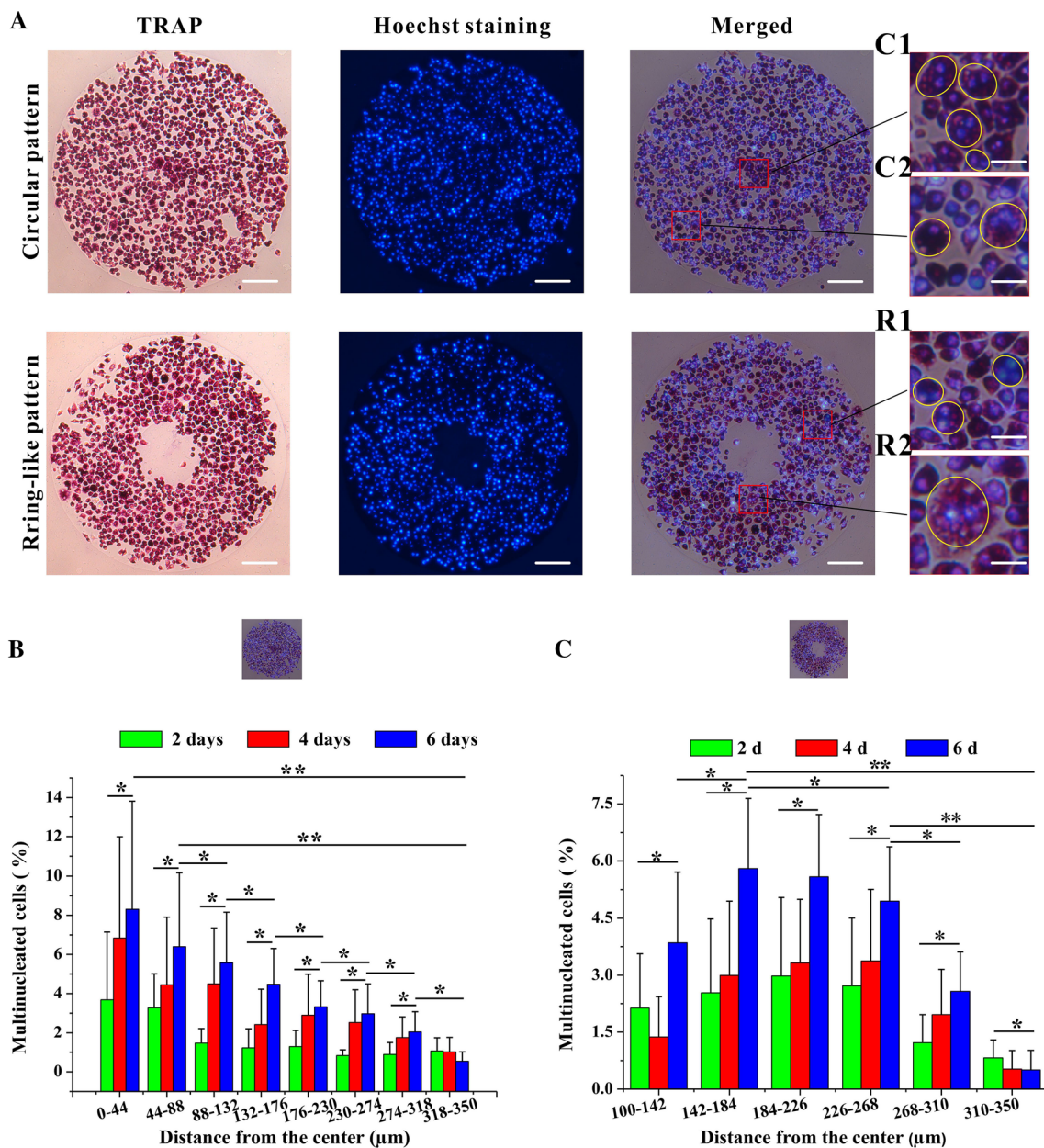


Fig. 2 Fusion of RAW264.7 cells on the micropatterned substrates. **a** TRAP and nuclear staining of RAW264.7 cells seeded on the circular and ring-like micropatterned substrates after 4-day induction. Yellow ovals represent the regions with MNCs. Scale bar for the entire pat-

terns, 100 μm; scale bar for insets C1, C2, R1, and R2, 30 μm. Percentage of MNCs at different distances away from the center of the circular (**b**) and ring-like (**c**) patterns after 2-, 4-, and 6-day induction. * $P < 0.05$; ** $P < 0.01$

performed to reveal the distribution of cell–substrate traction stress and in-plane maximal stress (Fig. 3). The results showed that the traction stress between the cell monolayer and the substrate was the highest in the outer edge of circular pattern and in the inner and outer edge regions of ring-like pattern (Fig. 3c). The circumferential stress σ_θ and radial stress σ_r in the cell monolayer were maximal at the edges of either circular or ring-like pattern. The in-plane maximal shear stress in the cell monolayer, $\tau_{\theta r}^{\max} = (\sigma_\theta - \sigma_r)/2$, had

the same tendency with traction stress, that is, the maximal values appearing at the edges. The above simulation results showed that the radial distribution of cell–substrate traction stress and in-plane maximal shear stress of cell monolayer was consistent with the radial distribution of cell fusion.

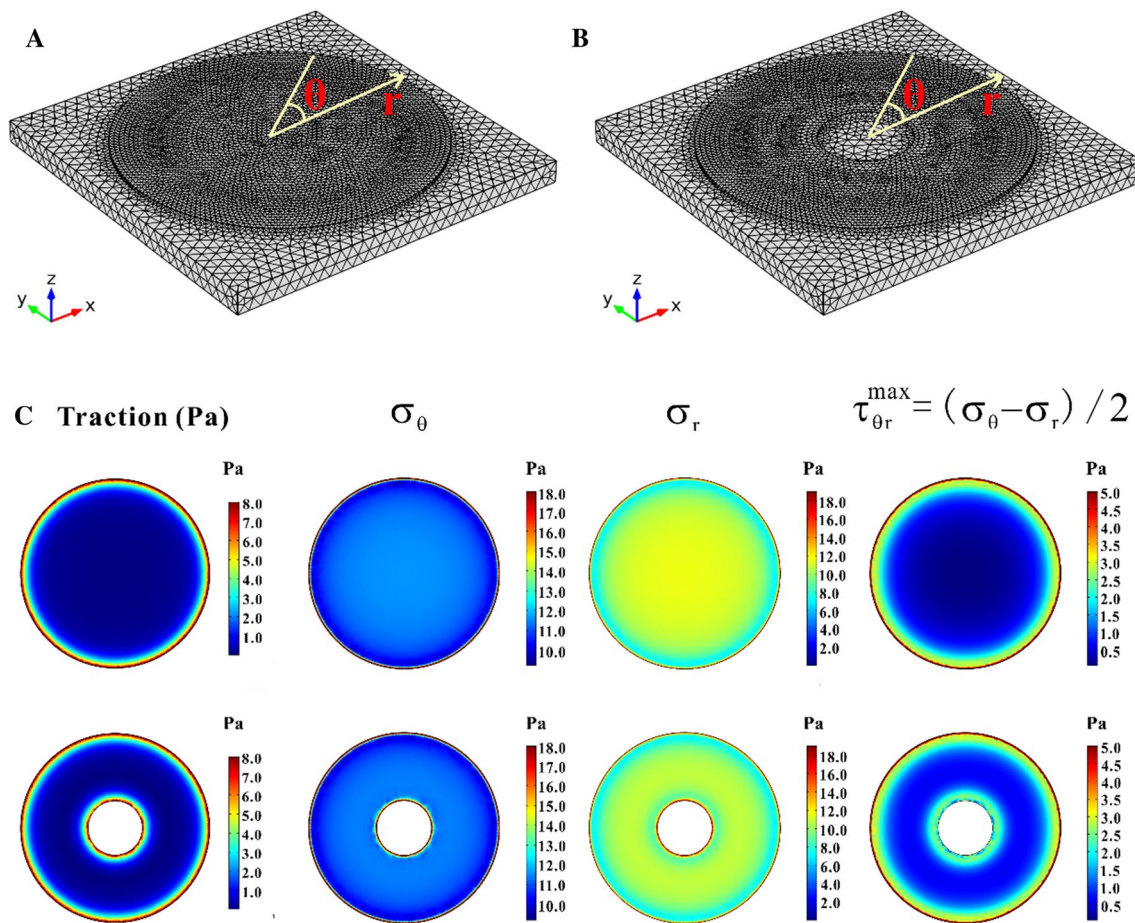


Fig. 3 Numerical simulation of the mechanical state in RAW264.7 cell monolayer on the circular and ring-like patterns. Mesh of finite element models for circular (a) and ring-like patterns (b). c Fringe

graph of traction stress between cell monolayer and substrate, circumferential and radial stresses, as well as in-plane maximal shear stress in cell monolayer, on the circular and ring-like patterns

3.3 Cell–substrate traction force is decided by the adhesion morphology of cell monolayer

To experimentally measure the mechanical state between cell monolayer and substrate, cell traction force was performed after RAW264.7 cells were cultured on the gel substrate with ring-like or circular pattern for 2, 4, or 6 days (Fig. 4). For the circular pattern group, the traction force increased with the distance away from the center (Fig. 4c), and the largest value appeared at the outer edge, that is, 55.5 Pa (2 days), 33.5 Pa (4 days), and 28.0 Pa (6 days). For the ring-like pattern group, the largest traction force occurred at the inner and outer regions, especially after the 6-day culture, which is consistent with the numerical result.

3.4 Distribution of mechanical force-transmitting molecules depends on the adhesion morphology

To investigate whether cells responded to the mechanical state, four types of mechanical force-transmitting molecules, namely F-actin, vinculin, β -catenin, and E-cadherin, were fluorescently stained when RAW264.7 cells were cultured on the ring-like pattern for 2 days. The results showed that F-actin was mainly distributed in the periphery of each cell, whereas vinculin, β -catenin, and E-cadherin existed inside the entire cell (Fig. 5a). Considering the distribution of these molecules in the cell monolayer, they were obviously abundant at the outer edge of the pattern. Statistical results showed that the fluorescent intensity in the outer region was significantly higher than that in the interior regions, indicating that the distribution of force-transmitting molecules may be induced by the mechanical state in the cell monolayer.

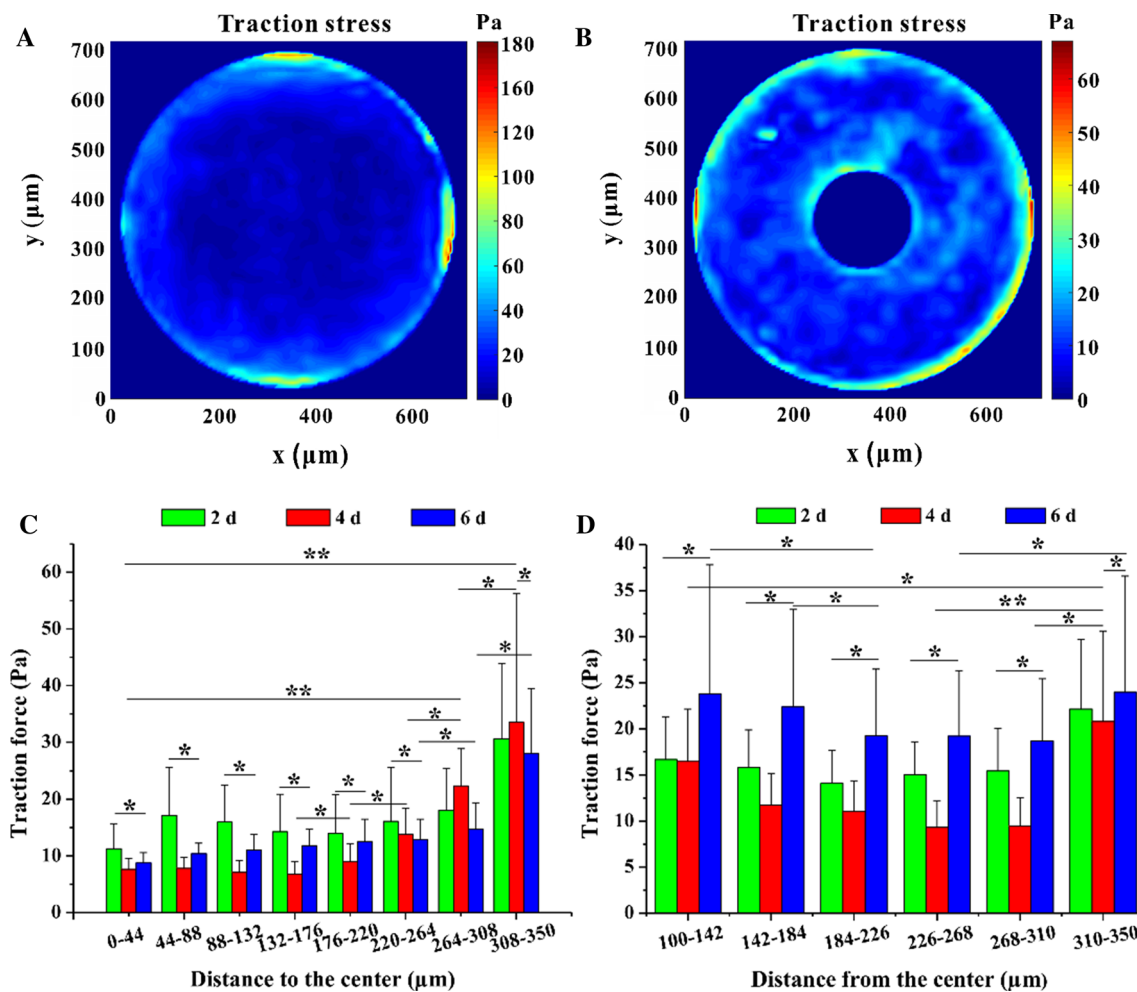


Fig. 4 Cell–substrate traction force measurement of RAW264.7 cells on the micropatterned substrate. Color maps of the measured traction force for circular (a) and ring-like (b) patterns for cells cultured for

4 days. Statistical analyses of traction force distribution at different locations away from the center for circular (c) and ring-like (d) patterns after 2-, 4-, and 6-day induction. * $P < 0.05$; ** $P < 0.01$

3.5 Cell–cell contact is necessary for the region-dependent cell fusion

We also studied the effect of seeding density of RAW264.7 cells on this region-dependent fusion for the ring-like pattern. For the HD group, cells aggregated together to form a monolayer as early as 2 days (Fig. 6a), whereas the cells of the LD group came into contact until 4 days (Fig. 6b). The cell density at different regions along the radial direction was used to quantitatively describe the cellular proliferation and distribution. The cell density within the entire pattern increased after seeding and maintained a plateau value of approximately 4000 cells/mm² after 2 days for HD and 3 days for LD (Fig. 6c). The cell density at different regions showed a limited dispersity and that at the interior distance such as 204 μm had a slightly lower value (Fig. 6d, e). Interestingly, 2 days after the cell monolayer formed in the HD group (Fig. 6a, d), the proportion of MNCs with more than 2

nuclei did not show a significant difference along the radial direction until the 4-day culture (Fig. 6f, g). The fusion proportion in the interior was 6.4–6.7%, which was twofold of those in the inner and outer regions (Fig. 6g). For the LD group, this region-dependent distribution of MNCs only appeared after 6-day culture (Fig. 6h). Clearly, the region-dependent distribution of MNCs occurred early in the HD group compared with the LD group (Figs. S1A and S1B), although the percentage of the MNCs with specific nuclear numbers did not show a difference between the HD and LD groups after 4- or 6-day induction (Figs. S1C and S1D). In addition, no significant difference for nuclear density was found in different regions along the radial direction, indicating that this region-dependent cell fusion was not due to cell aggregation in a specific region.

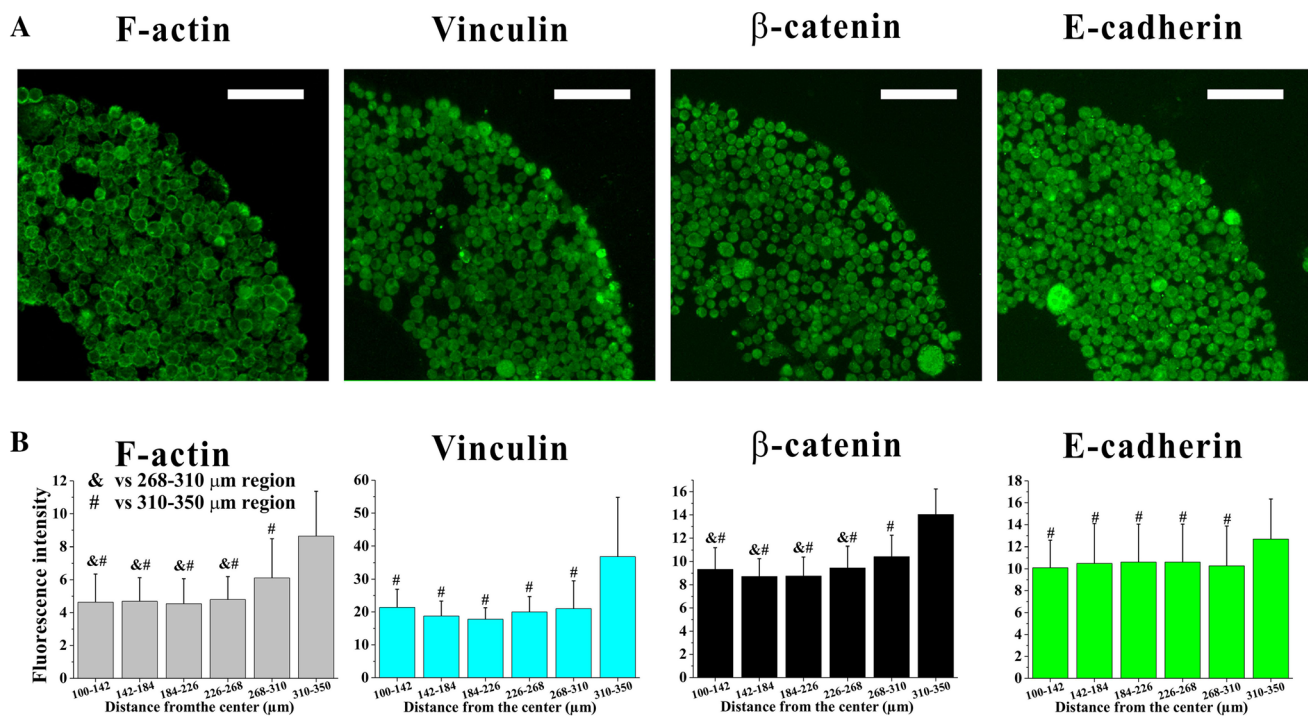


Fig. 5 Distribution of force-transmitting molecules for RAW264.7 cells cultured on the ring-like pattern for 2-day induction. **a** Fluorescent images of F-actin, vinculin, β -catenin, and E-cadherin of cells

seeded on the ring-like pattern. Scale bar, 100 μ m. **b** Histograms of fluorescence intensity of F-actin, vinculin, β -catenin, and E-cadherin at different locations away from the center. $\&\#p < 0.05$

3.6 Cadherin-related cell–cell interactions and induction medium regulate the region-dependent fusion

To further clarify whether this region dependence was decided by cell–cell connection, E-cadherin antibody and low-calcium medium were adopted to block intercellular interaction. After RAW264.7 monocytes were seeded with HD on the ring-like pattern for 4 days with low-calcium induction medium, the percentage of MNCs greatly decreased (Fig. 7b, e), but that in the interior was still higher than that in the inner or outer edges (Fig. S2). The MNC density with 2–4 nuclei was suppressed to approximately 50–100 cells/mm² (Fig. 7f), which was significantly lower than that of the control group at 100–200 cells/mm² (Fig. 7a). The MNC density with 5–7 nuclei decreased to 10–20 cells/mm². When we maintained 1 μ g/mL of anti-E-cadherin antibody (ECCD-1) in the induction medium during 4-day culture, the percentage of MNCs greatly decreased, and the region-dependent fusion disappeared (Fig. 7c, e). The MNC density with 2–4 nuclei was suppressed to approximately 50–100 cells/mm² and that with 5–7 nuclei decreased to 6–16 cells/mm² (Fig. 7g and S3). If no conditioned medium was added in the culture medium, only less than 1% of MNCs formed (Fig. 7d, e), and no significant difference along the radial direction was found. The

analysis of nuclear number showed that the MNC density with 2–4 nuclei was significantly suppressed to approximately 20–40 cells/mm² and that with 5–7 nuclei decreased to less than 10 cells/mm² (Fig. 7h).

4 Discussion

In this study, we examined the fusion of RAW264.7 monocytes cultured on the ring-like or circular pattern with induction medium for approximately 2, 4, or 6 days. The results showed that most of the MNCs were distributed in the interior regions (approximately 3.6% in 2 days, 3.5% in 4 days, and 5.6% in 6 days) for the ring-like pattern, which were significantly higher than those in the edge area (approximately 0.5%). For the circular pattern group, the highest proportion of the fusion occurred in the center region (approximately 3.6% in 2 days, 6.8% in 4 days, and 8.3% in 6 days), which were higher than those in the outer regions (approximately 2%). This phenomenon was also observed when we changed the inner radius of the ring-like pattern as 100, 150, or 200 μ m (Figs. S4B–S4E). The percentages of the MNCs at the interior reached up to 6% or more, which was higher than that at the edges (Fig. S4E). The above results imply that the fusion of MNCs tends to occur in the regions away from the edges of the cell monolayer.

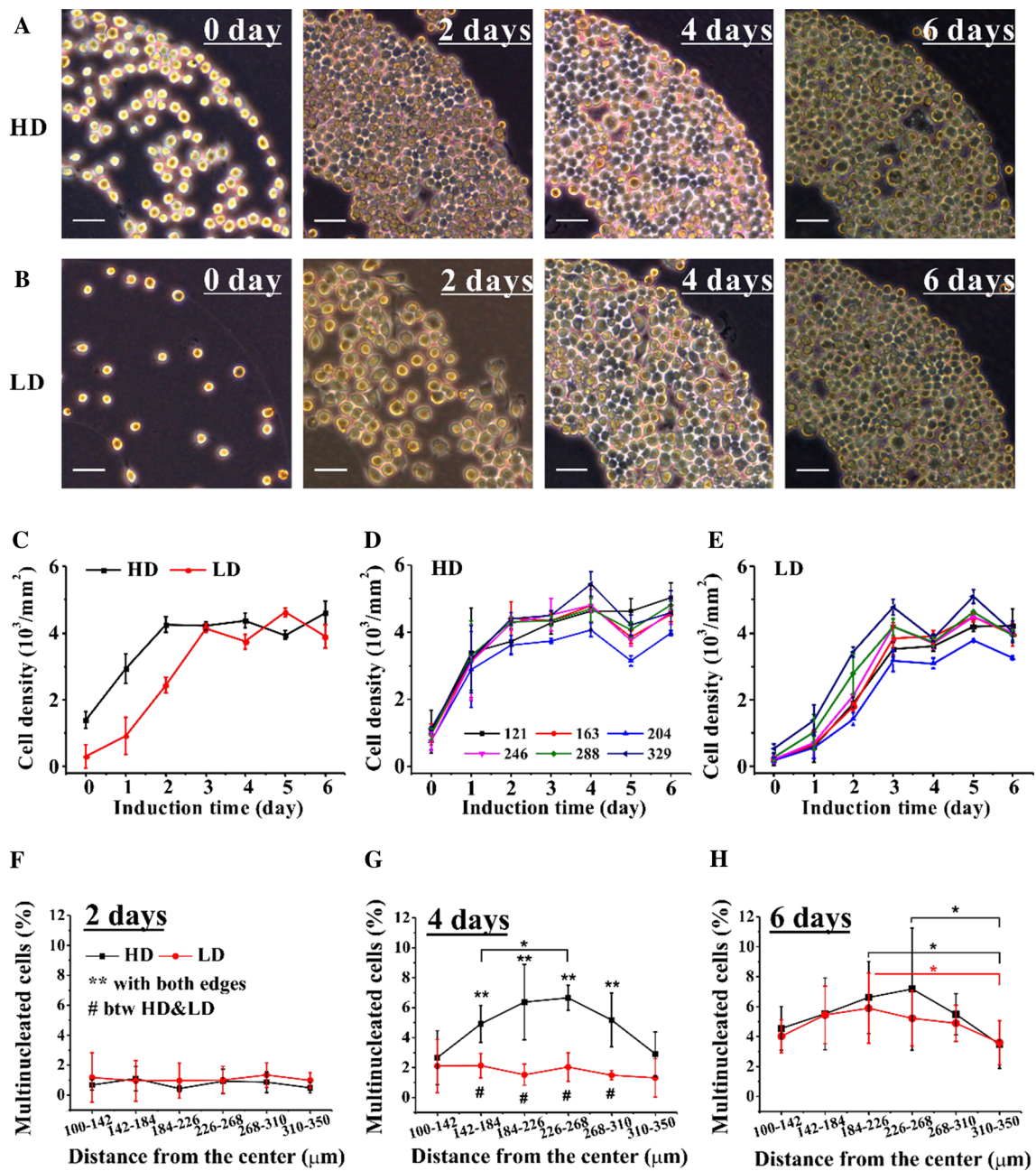


Fig. 6 Distribution of multinucleated osteoclasts on the ring-like pattern at different induction time periods for high and low seeding densities. Optical microscopic images of RAW264.7 cells seeded with high density (HD) (a) and low density (LD) (b) at different induction time periods. Cell density as a function of induction time in the entire

ring-like pattern (c) and in different regions for HD (d) and LD (e). Population percentage of multinucleated osteoclasts located in different regions on the ring-like pattern with different induction time periods: 2 days (f), 4 days (g), and 6 days (h). Scale bar, 50 μm

We performed numerical simulation to further investigate the disruption of traction force in the cell monolayer on the ring-like or circular pattern. The distribution of in-plane maximal shear stress of the pattern was high in the edge regions and low in the interior regions, which is consistent with distribution of osteoclast fusion. The results showed that the traction force was large in the edges but small in

the interior for both patterns. To determine whether the mechanical state of the cell monolayer was associated with this region-dependent cell fusion and consistent with the numerical simulation result, cell–substrate traction force was measured. The result showed that the largest force appeared at the edge of the circular or ring-like pattern and was considerably larger than the force in the interior regions, which

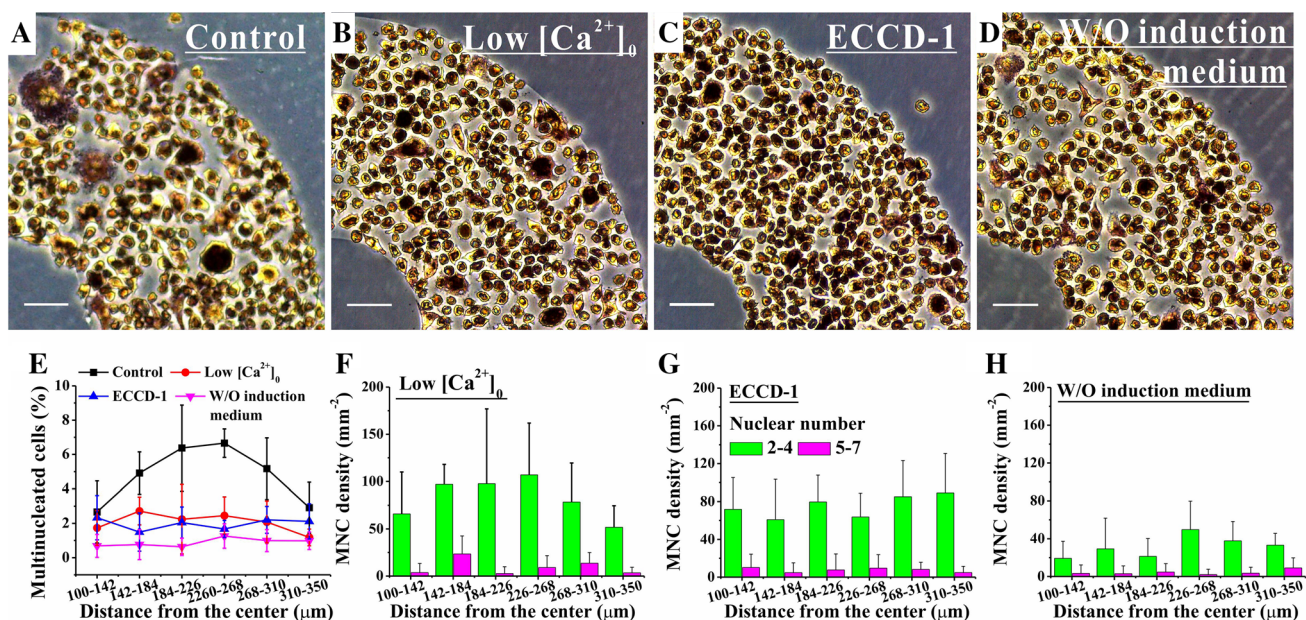


Fig. 7 Fusion of RAW264.7 cells on the ring-like pattern treated with anti-E-cadherin antibody (ECCD-1), low extracellular calcium medium (low $[Ca^{2+}]_0$), and no induction medium. TRAP staining

images (a–d), population percentage of multinucleated osteoclasts (e), and their density (f–h). Scale bar, 50 μ m

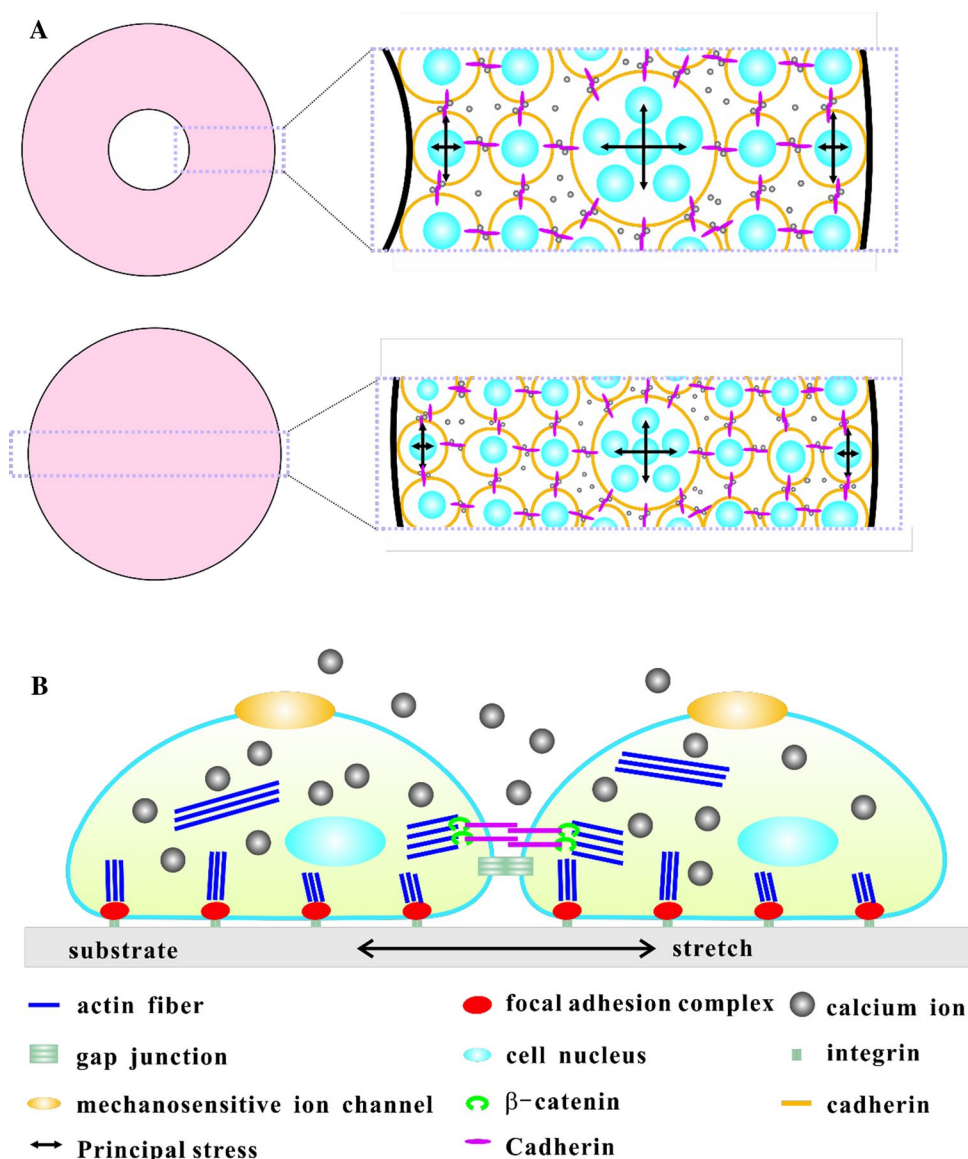
is consistent with the numerical result. However, the traction force at the outer edge region was slightly larger than that at the inner edge region. The reason may be that the curvature of the outer edge was less than that of the inner edge. Given that the lower level of traction force corresponded to higher cell fusion, the traction force in the cell monolayer may negatively regulate the fusion process of osteoclast precursors. Furthermore, the value of traction force obtained from the experimental measurement was approximately 20-fold of that from the numerical simulation, although their distribution along the radial direction was similar (Figs. 3c, 4a). This phenomenon may be because the cell–substrate interaction was dominated by the discrete focal adhesion complex, whose size was approximately 0.1–1 μ m (Kim and Wirtz 2013); therefore, cell–substrate stress should be concentrated around these complexes. This also explains why the distribution of traction stress in the experimental observation was not uniform like the numerical results. When the mechanical force-transmitting molecules of F-actin, vinculin, β -catenin, and E-cadherin were stained, their distribution showed a similar feature to that of the traction force, indicating that the cells at different positions were exposed to a region-dependent mechanical environment. In addition, the maximal traction force was less than 0.1 kPa in the present study, which was significantly lower than that of more than 2 kPa for osteoblasts MC3T3-E1 in our previous result (He et al. 2015). This may be due to the fact that MC3T3-E1 cells have strong cell–cell gap junctions, which has been

demonstrated by lots of studies (Plotkin and Bellido 2013; Guo et al. 2006).

After having been cultured on the micropatterned substrate, the density of cells at different regions showed a limited dispersity (Fig. 6d, e), suggesting that the proliferation and distribution of cells were uniform along the radial direction. The nuclear distribution (i.e., the distribution of RAW264.7 monocytes before fusion) was also uniform within the entire pattern, and the nuclear density along the radial direction did not display a region-dependent distribution (Fig. S1E and S1F). In the present study, most of the MNCs had 2–4 nuclei, and only less than 10% had 5–7 nuclei. The MNCs were demonstrated to be osteoclasts by staining them with TRAP (Fig. 2f), showing that most of the TRAP-positive multinucleated osteoclasts were located in the interior of the ring-like pattern.

The prerequisite condition of the region-dependent cell fusion is the formation of close intercellular contact in a cell monolayer. Hence, there are two key factors for cell fusion: seeding density and cell–cell connection. The primary factors regulating this process, that is, cell seeding density and the intercellular adhesive pathways such as extracellular calcium and E-cadherin, were investigated. When RAW264.7 monocytes were seeded with a very low density, they did not become confluent until 3-day induction (Fig. 6c, e), and the region-dependent fusion did not appear until 6-day induction (Fig. 6g, h). High seeding

Fig. 8 Schematic graph of the effect of cell–substrate and cell–cell interactions on cell fusion. **a** Cell–cell connection and cell fusion at different locations of the circular and ring-like patterns. **b** Side view of cell–cell and cell–substrate connections, as well as the corresponding molecules



density enhanced the confluence of cells and the region-dependent fusion (Fig. 6d, g), demonstrating that cell–cell contact is necessary for cell fusion. When cell–cell contact occurred for HD seeding or long-term culture, the cells in the interior region tended to be pulled by the surrounding cells, but the cells in the edge region exerted higher circumferential stretching forces from the neighboring cells (Fig. 8a, b). When the medium with less calcium ions or E-cadherin monoclonal antibody (ECCD-1) was used to inhibit the cell–cell connection via the calcium-dependent adhesion molecule of E-cadherin (Figs. S2 and S3), the region-dependent fusion was significantly

suppressed (Fig. 7e). This result is consistent with previous studies (Mbalaviele et al. 1995; Moreno et al. 2007), in which anti-E-cadherin antibody inhibited the formation of MNCs.

Based on the present results, we conclude that this region-dependent fusion behavior is due to the non-uniform distribution of mechanical force in the cell monolayer. The pattern of substrate on which the cell monolayer adheres may influence the calcium-dependent cell–cell connection, which then regulates the fusion process of osteoclast precursors. However, the detailed mechanism about the force transmitting between cell–substrate,

cell–cell, and intracellular cytoskeleton still needs further investigations.

Acknowledgements This work was supported by the National Natural Science Foundation of China [11572043 and 11372043 (BH)].

Author Contributions BH designed the research. QS performed the traction force experiment and numerical simulation, finalized the manuscript. CLL found the phenomenon on first and drafted the first version of manuscript. XB performed the experiments of force-transferring molecules and of cell fusion on circular pattern.

Compliance with Ethical Standards

Conflict of interest We declare that we have no conflicts of interest.

References

- Anderegge F, Geblinger D, Horvath P, Charnley M, Textor M, Addadi L, Geiger B (2011) Substrate adhesion regulates sealing zone architecture and dynamics in cultured osteoclasts. *PLoS ONE* 6:e28583
- Fu R, Liu Q, Song G, Baik A, Hu M, Sun S, Guo XE, Long M, Huo B (2013) Spreading area and shape regulate apoptosis and differentiation of osteoblasts. *Biomed Mater* 8:055005
- Gautrot JE, Wang C, Liu X, Goldie SJ, Trappmann B, Huck WT, Watt FM (2012) Mimicking normal tissue architecture and perturbation in cancer with engineered micro-epidermis. *Biomaterials* 33:5221–5229
- Guo XE, Takai E, Jiang X, Xu Q, Whitesides GM, Yardley JT, Hung CT, Chow EM, Hantschel T, Costa KD (2006) Intracellular calcium waves in bone cell networks under single cell nanoindentation. *Mol Cell Biomech* 3:95–107
- Hashimoto H, Munro E (2018) Dynamic interplay of cell fate, polarity and force generation in ascidian embryos. *Curr Opin Genet Dev* 51:67–77
- He SJ, Su YW, Ji BH, Gao HJ (2014) Some basic questions on mechanosensing in cell–substrate interaction. *J Mech Phys Solids* 70:116–135
- He S, Liu C, Li X, Ma S, Huo B, Ji B (2015) Dissecting collective cell behavior in polarization and alignment on micropatterned substrates. *Biophys J* 109:489–500
- Helming L, Gordon S (2009) Molecular mediators of macrophage fusion. *Trends Cell Biol* 19:514–522
- Kilian KA, Bugarija B, Lahn BT, Mrksich M (2010) Geometric cues for directing the differentiation of mesenchymal stem cells. *Proc Natl Acad Sci USA* 107:4872–4877
- Kim DH, Wirtz D (2013) Focal adhesion size uniquely predicts cell migration. *FASEB J* 27:1351–1361
- Kim J, Bae WG, Choung HW, Lim KT, Seonwoo H, Jeong HE, Suh KY, Jeon NL, Choung PH, Chung JH (2014) Multiscale patterned transplantable stem cell patches for bone tissue regeneration. *Biomaterials* 35:9058–9067
- Kozlov MM, McMahon HT, Chernomordik LV (2010) Protein-driven membrane stresses in fusion and fission. *Trends Biochem Sci* 35:699–706
- Li P, Hu M, Sun S, Zhang Y, Gao Y, Long M, Huo B, Zhang D (2012) Fluid flow-induced calcium response in early or late differentiated osteoclasts. *Ann Biomed Eng* 40:1874–1883
- Liu CL, He SJ, Li XJ, Huo B, Ji BH (2016) Mechanics of cell mechanosensing on patterned substrate. *J Appl Mech Trans ASME* 83:8
- Ma HW, Hyun J, Zhang ZP, Beebe TP, Chilkoti A (2005) Fabrication of biofunctionalized quasi-three-dimensional microstructures of a nonfouling comb polymer using soft lithography. *Adv Func Mater* 15:529–540
- Mbalaviele G, Chen H, Boyce BF, Mundy GR, Yoneda T (1995) The role of cadherin in the generation of multinucleated osteoclasts from mononuclear precursors in murine marrow. *J Clin Invest* 95:2757–2765
- McBeath R, Pirone DM, Nelson CM, Bhadriraju K, Chen CS (2004) Cell shape, cytoskeletal tension, and RhoA regulate stem cell lineage commitment. *Dev Cell* 6:483–495
- Merle T, Farge E (2018) Trans-scale mechanotransductive cascade of biochemical and biomechanical patterning in embryonic development: the light side of the force. *Curr Opin Cell Biol* 55:111–118
- Moreno JL, Mikhailenko I, Tondravi MM, Keegan AD (2007) IL-4 promotes the formation of multinucleated giant cells from macrophage precursors by a STAT6-dependent, homotypic mechanism: contribution of E-cadherin. *J Leukoc Biol* 82:1542–1553
- Nelson CM, Jean RP, Tan JL, Liu WF, Sniadecki NJ, Spector AA, Chen CS (2005) Emergent patterns of growth controlled by multicellular form and mechanics. *Proc Natl Acad Sci USA* 102:11594–11599
- Plotkin LI, Bellido T (2013) Beyond gap junctions: Connexin43 and bone cell signaling. *Bone* 52:157–166
- Robert J, Pelham J, Wang YL (1997) Cell locomotion and focal adhesions are regulated by substrate flexibility. In: *Proceedings of the national academy of sciences of the United States of America*, pp 13661–13665
- Ruiz SA, Chen CS (2008) Emergence of patterned stem cell differentiation within multicellular structures. *Stem Cells* 26:2921–2927
- Shillcock JC, Lipowsky R (2005) Tension-induced fusion of bilayer membranes and vesicles. *Nat Mater* 4:225–228
- Vuong-Brender TT, Ben Amar M, Pontabry J, Labouesse M (2017) The interplay of stiffness and force anisotropies drives embryo elongation. *Elife* 6(e23866):1–9
- Wan LQ, Kang SM, Eng G, Grayson WL, Lu XL, Huo B, Gimble J, Guo XE, Mow VC, Vunjak-Novakovic G (2010) Geometric control of human stem cell morphology and differentiation. *Integr Biol* 2:346–353

Publisher's Note Springer Nature remains neutral with regard to jurisdictional claims in published maps and institutional affiliations.